

Fragmentation at the Earliest Phase of Massive Star Formation

Qizhou Zhang, Yang Wang, Thushara Pillai, Jill Rathborne

Harvard-Smithsonian Center for Astrophysics, 60 Garden Street, Cambridge, MA 02138

qzhang@cfa.harvard.edu

ABSTRACT

We present 1.3mm continuum and spectral line images of two massive molecular clumps P1 and P2 in the G28.34+0.06 region with the Submillimeter Array. While the two clumps contain masses of 1000 and 880 M_{\odot} , respectively, P1 has a luminosity $< 10^2 L_{\odot}$, and a lower gas temperature and smaller line width than P2. Thus, P1 appears to be at a much earlier stage of massive star formation than P2. The high resolution SMA observations reveal two distinctive cores in P2 with masses of 97 and 49 M_{\odot} , respectively. The 4 GHz spectral bandpass captures line emission from CO isotopologues, SO, CH₃OH, and CH₃CN, similar to hot molecular cores harboring massive young stars. The P1 clump, on the other hand, is resolved into five cores along the filament with masses from 22 to 64 M_{\odot} and an average projected separation of 0.19 pc. Except ¹²CO, no molecular line emission is detected toward the P1 cores at a 1σ rms of 0.1 K. Since strong ¹²CO and C¹⁸O emissions are seen with the single dish telescope at a resolution of 11", the non-detection of these lines with the SMA indicates a depletion factor upto 10^3 . While the spatial resolution of the SMA is better than the expected Jeans length, the masses in P1 cores are much larger than the thermal Jeans mass, indicating the importance of turbulence and/or magnetic fields in cloud fragmentation. The hierarchical structures in the P1 region provide a glimpse of the initial phase of massive star and cluster formation.

Subject headings: clouds - ISM: kinematics and dynamics -stars: formation

1. Introduction

In the past decade, significant progress has been made toward understanding the more evolved stages of massive star formation, phases from hot molecular cores to hyper compact HII regions. It becomes clear that massive proto B stars are associated with molecular outflows and rotating disks (Cesaroni et al. 1997; Zhang et al. 1998, 2001; Beuther et al. 2002).

Therefore, they likely form through a disk mediated accretion (Zhang 2005; Cesaroni et al. 2007). Active mass accretion can continue during the hyper compact HII region phase when the ionization radius is within the gravitational radius (Keto 2002a,b; Sollins et al. 2005). All these studies represents phases of massive star formation after the central star has formed and begun hydrogen burning. Contrary to these progresses, little is known about the initial phases of massive star formation. Since most massive stars are born in a cluster environment (Lada & Lada 2003), the initial phase of massive star formation is intimately linked to cluster formation and the fragmentation of molecular clouds. While theoretical work provides physical insights into fragmentation process, direct observations of precluster molecular clouds are crucial in revealing how the process may take place. Among all the observational efforts, studies of infrared dark clouds (IRDC), massive clouds at extremely early stages of evolution, hold great promise and has grown rapidly over the past several years.

IRDCs were first discovered in large number by the Infrared Space Observatory (ISO) and the Midcourse Space Experiment (MSX) (Egan et al. 1998; Carey et al. 1998, 2000; Hennebelle et al. 2001; Simon et al. 2006b,a) through infrared absorption against the bright galactic background. Systematic studies found that many IRDCs contain over $10^3 M_{\odot}$ of dense molecular gas (Simon et al. 2006a; Rathborne et al. 2006; Pillai et al. 2006). While some massive IRDCs show signs of massive star formation through H_2O maser emission (Wang et al. 2006), CH_3OH maser emission (Ellingsen 2006), molecular outflows (Beuther & Sridharan 2007), and bright $24 \mu m$ emission (Rathborne et al. 2005), a large majority do not show signs of star formation (Wang et al. 2006). With a typical star formation efficiency, the large amount of dense gas in these IRDCs makes them the natural birth place for massive stars and clusters. Thus, these regions are premium sites for uncovering the initial conditions of massive star and cluster formation.

Wang et al. (2008) imaged an IRDC G28.34+0.06 with the Very Large Array in the NH_3 (1,1) and (2,2) lines in the D configuration. An overview of the region is presented in Figure 1. The cloud, at a distance of ~ 4.8 kpc, contains several $10^3 M_{\odot}$ of dense gas along the infrared absorption filament extending 6 pc in the sky (Carey et al. 2000; Rathborne et al. 2006; Pillai et al. 2006). Two prominent dust continuum clumps, P1 and P2, are revealed in the 850 and 450 μm images obtained from the JCMT (Carey et al. 2000) and the 1.2mm image obtained from the IRAM 30m telescope (Rathborne et al. 2006). Despite the fact that two clumps contain a similar amount of dense gas within 0.3 pc, the P2 region has a high gas temperature of 30 K, large NH_3 line width of 3.3 km s^{-1} and is associated with a strong $24 \mu m$ point source with far IR luminosity of $10^3 L_{\odot}$. This is in contrast to P1 which has a gas temperature of 13 K, a relatively narrow NH_3 line width of 1.7 km s^{-1} , and an upper limit to the luminosity of $10^2 L_{\odot}$ (Wang et al. 2008). Furthermore, the gas in P1 appears to be externally heated with temperatures decreasing from 20 K in the outside of the cloud to

13 K inside of the cloud. Likewise, the turbulence measured by the NH_3 line widths appears to decrease from larger spatial scales to smaller scales. These observations led Wang et al. (2008) to suggest that P1 is at a much earlier stage of massive star formation compared to P2.

In order to study the cloud structure, we imaged the P1 and P2 clumps at $\sim 1''$ resolution with the SMA. The sensitive continuum image at 1.3mm reveals 5 dense cores toward the P1 clump. The P2 region exhibits rich molecular line emission similar to hot molecular cores, while the P1 cores are absent of molecular line emission, which indicates heavy depletion.

2. Observations

Observations with the SMA¹ were carried out with 7 antennas in the compact configuration on 2006 August 07, and 8 antennas in the extended configuration on 2008 July 22. The pointing centers of the observations were RA (J2000) = 18:42:52.09, Dec (J2000) = -3:59:52.00 for P2 and RA (J2000) = 18:42:50.74, Dec (J2000) = -04:03:15.34 for P1. The FWHM of the primary beam of the two pointings is shown as the dashed circles in Figure 1.

For the compact configuration, quasars 1741-038 and 1908-201 were used as time dependent gain calibrators, Uranus and Ganymede were used as bandpass and flux calibrators, respectively. The system temperatures during the observations varied from 200 to 600 K. The receivers were tuned to an LO frequency of 225 GHz. With IF frequencies of 4–6 GHz, the observations covered rest frequencies from 220 through 222 GHz in the LSB, and 230 through 232 GHz in the USB, with a uniform channel spacing of 0.8125 MHz ($\sim 1 \text{ km s}^{-1}$) across the entire band.

For observations with the extended configuration, we used 1751+096 and 1911-201 as gain calibrators, 3C279 and 3C454.3 as bandpass calibrators, and Callisto as a flux calibrator. The system temperatures during the observations were around 100 K. The receivers were tuned to an LO frequency of 220 GHz and covered rest frequencies of 215.7 through 217.7 GHz in the LSB, and 225.7 through 227.7 GHz in the USB, with a uniform channel spacing of 0.4062 MHz ($\sim 0.5 \text{ km s}^{-1}$) across the entire band. A detailed description of the SMA is given in Ho et al. (2004).

The visibility data were calibrated with the IDL superset MIR package developed for

¹The Submillimeter Array is a joint project between the Smithsonian Astrophysical Observatory and the Academia Sinica Institute of Astronomy and Astrophysics, and is funded by the Smithsonian Institution and the Academia Sinica.

the Owens Valley Interferometer. The absolute flux level is accurate to about 15%. After the calibration in MIR, the visibility data were exported to the MIRIAD format for further processing and imaging. The continuum is constructed from line free channels in the visibility domain. The projected baselines range from 12 to 68 m in the compact configuration, and 20 to 221 m in the extended configuration. We combined the continuum data from both configurations, which yields a synthesized beam of about $1.2''$, and a 1σ rms of 1 mJy in the naturally weighted maps. The spectral line data presented here is from the compact configuration only, with a 1σ rms of 90 mJy beam $^{-1}$ per 1.2 km s $^{-1}$ channel, and a spatial resolution of $3''$. The uncertainty in the absolute position is $\lesssim 0''.2$, derived from comparing the secondary gain calibrators with their catalog positions.

3. Results and Discussions

3.1. Continuum Emission

Figure 2 presents the 1.2mm continuum emission from the IRAM 30m telescope (Rathborne et al. 2006), the NH $_3$ (1,1) emission from the VLA (Wang et al. 2008), and the SMA 1.3mm dust continuum emission. To describe the dust emission, we follow the nomenclature in the literature that *clumps* refer to structures with sizes of ~ 1 pc, *cores* refer to structures within a clump with sizes of ~ 0.1 pc, and *condensations* refer to sub structures within a core. As shown in Figure 2, the two dust clumps P1 and P2 detected with the IRAM 30m telescope and JCMT at resolutions from $11''$ to $15''$ (Rathborne et al. 2006; Carey et al. 1998) are resolved by the SMA into multiple structures at $1''.2$ resolution. The P1 clump splits into five cores (P1-SMA1, P1-SMA2, P1-SMA3, P1-SMA4 and P1-SMA5) with an average projected separation of $8''$ or 0.19 pc. These cores show further substructures that may correspond to condensations. Since we do not have complementary spectral line data at a resolution of $1''$, we defer analysis of the substructure to a future paper. The emission in P2, on the other hand, is resolved into two strong, distinctive cores, P2-SMA1 and P2-SMA2. H $_2$ O masers reported in Wang et al. (2006) coincide with P1-SMA2 and P2-SMA2 to within $0.1''$.

The continuum images from the SMA and the IRAM 30m telescope are in a remarkably good agreement with the NH $_3$ emission. The five continuum cores (P1-SMA1 through P1-SMA5) lie along the NH $_3$ ridge. There is a feature in the 30-m continuum image extending toward another NH $_3$ peak in the northwest. The SMA image from the compact configuration reveals a peak at 5 mJy (4σ). This peak is not detected in the $1''.2$ resolution image presented in Figure 2.

The 1.2mm integrated flux densities from the IRAM 30m telescope are 2.6 Jy and 1.3

Jy, toward P2 and P1, respectively. Neither clumps have detectable continuum emission at centimeter wavelength at a level of 1 mJy (Wang et al. 2008), thus the mm flux arises predominantly from the dust emission. Using the dust opacity of Hildebrand (1983), an emissivity index of $\beta = 1.5$, and a temperature of 13 and 30 K derived from NH_3 (Wang et al. 2008), we obtained dust mass of 1000 and 880 M_\odot for P1 and P2, respectively, with an average H_2 density of $3 \times 10^5 \text{ cm}^{-3}$. The masses in the P1 and P2 clumps are consistent with the estimate in Carey et al. (2000) from 850 μm and 450 μm if one factors in the different values of dust temperatures used. For $\beta = 2$ as assumed in Rathborne et al. (2006), we obtain a mass of 2000 and 1760 M_\odot for the P1 and P2 clumps, respectively.

We measure the flux density toward the dust cores in the SMA images. For the P2 cores, the integrated fluxes were obtained from fits of elliptical Gaussian. For the P1 cores, we derived the integrated fluxes within a polygon encompassing each core. The peak positions and the integrated fluxes are listed in Table 1. The NH_3 (1,1) and (2,2) data reveal gas temperatures of 13 to 16 K in cores toward P1, and 30 K in cores toward P2. Using the same dust opacity law and a dust emissivity index of $\beta = 1.5$, appropriate for massive dense cores based on multi-wavelength observations at mm and submm wavelengths (Beuther et al. 2007), we obtained dust masses for the cores ranging from 22 to 97 M_\odot . The corresponding H_2 densities in these cores range from 10^6 to 10^7 cm^{-3} . These parameters are also listed in Table 1.

3.2. Line Spectra and Depletion

Figure 3 shows the spectra over the 4 GHz bandpass of the SMA toward P2-SMA1, and the strongest core, P1-SMA4, in the P1 clump. The spectra are made from the compact configuration with a resolution of $3'' - 4''$. Toward P2-SMA1, emissions of CO isotopologues, SO, and more complex molecules CH_3OH , H_2^{13}CO , HNC, as well as CH_3CN are detected. The presence of complex organic molecule is similar to that of hot cores observed with the SMA (Beuther et al. 2005; Zhang et al. 2007; Rathborne et al. 2008). The classical hot core molecule CH_3CN is detected in the $K=0, 1, 2, 3,$ and 4 components of the $J=12-11$ transition. Physical parameters, namely, column density and temperature, have been estimated by fitting CH_3CN spectrum, in the LTE approximation, and taking into account the optical depth effect. The best fit gives a temperature of 120 K, representative of the temperature value in a typical hot core.

In contrast to the rich line spectra in P2-SMA1, no molecular line emission except the faint ^{12}CO 2-1 emission is detected toward P1-SMA4. One can estimate CO depletion from the 2-1 emission of the CO isotopologues. Toward the P2 position, the ^{13}CO to C^{18}O ratio

yields an optical depth of 1.8 in the ^{13}CO 2-1 line assuming a $[\text{C}^{13}\text{CO}/\text{C}^{18}\text{O}]$ of 40. We use the C^{18}O 2-1 transition to estimate the CO column density because it is optically thin, and is least affected by missing short spacing in the SMA data as compared to ^{13}CO and ^{12}CO . With a brightness temperature of 2.5K, a FWHM of 2.5 km s^{-1} in the C^{18}O 2-1 line width, and a gas temperature of 30K, we obtain a ^{12}CO column density of $4 \times 10^{14} \text{ cm}^{-2}$, assuming a $[\text{C}^{12}\text{CO}/\text{C}^{18}\text{O}]$ of 240. On the other hand, the H_2 column density derived from the dust emission, assuming a dust to gas ratio of 1:100 amounts to $8 \times 10^{23} \text{ cm}^{-2}$. These values give rise to a $[\text{CO}/\text{H}_2]$ ratio of 1.2×10^{-6} , a factor of 100 lower than the standard value of 10^{-4} in $[\text{CO}/\text{H}_2]$ ratio.

Similarly, one can estimate CO depletion from the upper limit of 0.1K in the C^{18}O 2-1 line in P1-SMA4. If the C^{18}O 2-1 emission is optically thin, the 0.1 K upper limit and the 13K gas temperature yield a ^{12}CO column density of $2.2 \times 10^{16} \text{ cm}^{-2}$. The 1.3 continuum emission gives rise to an H_2 column density of $2.1 \times 10^{23} \text{ cm}^{-2}$. Therefore, we obtain a $[\text{CO}/\text{H}_2]$ ratio of $\sim 10^{-7}$, or a CO depletion of 10^3 from the standard $[\text{CO}/\text{H}_2]$ ratio.

The non detection of molecular line emission with the SMA is in staunch contrast with the strong line emission in CO isopologues, CS, HCN toward P1 with the IRAM 30m telescope (Rathborne personal communication). The brightness temperatures of the ^{13}CO and C^{18}O 2-1 lines are 3 and 1 K, respectively. The line ratio yields an optical depth in ^{13}CO of 2. With a gas temperature of 16 K from the single dish NH_3 (Pillai et al. 2006) and a brightness temperature of 1K in the C^{18}O 2-1 line, we obtain a column density of $7.5 \times 10^{17} \text{ cm}^{-2}$ in ^{12}CO . The H_2 column density, based on the measurement from the IRAM 30m telescope at 1.2mm is $3 \times 10^{23} \text{ cm}^{-2}$. These values yield a $[\text{CO}/\text{H}_2]$ ratio of 2.5×10^{-6} , which is 40 times lower than the typical value (10^{-4}) in the Galaxy. Pillai et al. (2007) reported a similar results in the $[\text{CO}/\text{H}_2]$ ratio toward this region.

The estimates above yield CO depletion upto 10^2 to 10^3 in P2 and P1, respectively. It is known that carbon bearing molecules such as CO are heavily depleted in low-mass prestellar cores (Bergin & Tafalla 2007). This phenomenon is seen in massive cores over a scale of nearly 0.1 pc, much larger than the 10^3 AU scale in the low-mass prestellar cores. The timescale of depletion for an average density of 10^5 cm^{-3} is several 10^4 yrs (Bergin & Tafalla 2007). This timescale sets a lower limit to the age of the P1 cores at $> 10^5$ years.

3.3. Core Structure and Dynamical State

The dust emission from the SMA observations appears to be centrally peaked. For a core internally heated by a protostar, the dust temperature scales as $T_{dust} \propto r^{-a}$ (Scoville & Kwan

1976) with $a = 0.33$. If the core density ρ scales as r^{-b} , then the flux density from dust emission $F \propto \int \rho T_{dust} ds$, where s is the length along the line of sight. When $a + b > 1$, we find $F \propto r^{-(a+b-1)}$. The Fourier transform of the flux density becomes $A \propto S_{uv}^{(a+b-3)}$ (Looney et al. 2000; Beuther et al. 2007), where A is the visibility amplitude and $S_{uv} = \sqrt{(u^2 + v^2)}$ is the UV distance.

Figure 4 presents the density profile for P2-SMA1, and P1-SMA4, two of the strongest cores in the clumps. The visibility is vector averaged over concentric annuli around the center of the core. The least-squared fit to visibilities yields $b = 1.6 \pm 0.2$ for P2-SMA1, and $b = 2.1 \pm 0.2$ for P1-SMA4, if $a = 0.33$. The visibility data toward the P1-SMA4 have larger scatters due to a limited signal-to-noise ratio, thus the uncertainty to the power-law index is larger than the statistical error quoted here.

The density profiles in both P1 and P2 cores are consistent with a power law relation r^{-b} with b between 1.5 to 2, similar to those found in hot molecular cores (van der Tak et al. 2000). Such power law structures suggest that these cores may be evolved from an equilibrium state. A self gravitating core in a hydrostatic equilibrium has a density structure of r^{-2} . A hydrostatic core truncated by external pressure, *i.e.*, the Bonnor-Ebert sphere has a similar density structure in the outer radii with a flatter inner profile. These density structures have been found in low-mass prestellar cores (Alves et al. 2001). The fact that the more massive cores in the G28 region shows similar structures is rather intriguing, and suggests that cores may evolve slowly to allow them reaching a quasistatic equilibrium state. This is consistent with the age of the cores inferred from the time scale of chemical depletion.

3.4. Core Fragmentation and Cluster Formation

The early evolutionary stage of the P1 clump makes it an excellent target to study the initial fragmentation in molecular clouds. The structures revealed by the high resolution SMA observations are consistent with a hierarchical fragmentation of molecular clouds. It appears that the initial fragmentation gives rise to 5 massive cores with masses from 22 to 64 M_{\odot} with an average separation of $8''$ or 0.19 pc. The cores appear to further fragment as core densities continue to increase. The average density in the P1 clump based on the IRAM 30m telescope is $3 \times 10^5 \text{ cm}^{-3}$. With an average gas temperature in the clump of 16 K, we find a Jeans mass of 1 M_{\odot} and a Jeans length of 0.05 pc. Despite the fact that the SMA observations spatially resolve the Jeans length, the core masses are more than a factor of 10 larger than the thermal Jeans mass. The large discrepancy between the Jeans mass and the observed core mass indicates that cloud fragmentation may not be controlled solely by the thermal pressure and gravity. Other stabilizing factors are required to account for the large

mass observed. Wang et al. (2008) reported a systematic decrease in the NH_3 line width from large scales to small scales of $3'' - 4''$, which cannot be attributed to organized motion. This decrease in line widths is interpreted as a turbulence decay in dense molecular gas. The observed NH_3 line width in the P1 cores is 1.7 km s^{-1} , a factor of 8 larger than the thermal line width. This supersonic turbulence likely plays an important role in fragmentation. The Virial masses measured from the NH_3 line widths are 103 and $24 M_\odot$ in P2 and P1 cores, respectively. The general agreement between the Virial mass and gas mass lends support to the notion that turbulence dominates fragmentation. In addition to turbulence, magnetic fields may also play a role in suppressing fragmentation. However, without direct measurements of field strengths, it is difficult to assess its importance relative to turbulence.

Several theoretical ideas postulate how massive star and cluster formation may begin. Observations find that massive stars and clusters form in higher density and more turbulent regions of molecular clouds as compared to their low mass counterparts. Bonnell & Bate (2002) propose in the competitive accretion model that clouds fragment initially into cores of Jeans mass of $\sim 0.5 M_\odot$. These cores subsequently form low-mass protostars that accrete the distributed gas from a reservoir of material in the molecular clump. Protostars located near the center of the gravitational potential accrete at a higher accretion rate because of a stronger gravitational pull, thus, experience a faster mass growth. This competitive accretion model reproduces the stellar IMF observed (Bonnell et al. 2004).

Alternatively, McKee & Tan (2002) propose a turbulent accretion model, in which stars form via a monolithic collapse of a molecular cloud. The heating from the embedded protostars increases the gas temperature, and thus, the Jeans mass. Therefore, the core mass function is similar to the stellar IMF (Krumholz et al. 2005, 2007).

The observed core masses in P1 appear to be much larger than the core mass assumed in the competitive accretion model (Bonnell & Bate 2005). The 3σ mass sensitivity of $2.5 M_\odot$ in this study does not detect the $0.5 M_\odot$ Jeans cores. However, the SMA observations have a spatial resolution better than the Jean length (0.05pc) predicted in the initial fragmentation. The fact that the core masses are much larger than the Jeans mass points to an inconsistency with the theoretical model. In addition, these cores do not represent transient objects because of the large masses, high average densities $> 10^6 \text{ cm}^{-3}$, and heavy chemical depletion. On the other hand, the mechanism of increasing Jeans mass through stellar heating proposed by Krumholz et al. (2005); Krumholz (2006) does not appear to be sufficient. To reach a Jeans mass of $30 M_\odot$ at a density of 10^5 cm^{-3} requires a gas temperature of 100K . This temperature is a factor of 7 times larger than the gas temperature derived from the NH_3 emission. Therefore, the increase in temperature is insufficient to stop fragmentation in the P1 region. The observations indicate that turbulence plays a crucial role in shaping

fragmentation in clouds. It has been suggested that turbulence dissipates rapidly and may not be sufficient to support cores at small scales. The NH_3 data from the VLA observations (Wang et al. 2008) demonstrate that despite turbulence decay, the line widths measured at $3'' - 4''$ scales appear to be large enough to support the cores in P1.

The core mass in the P2 clump is approximately a factor of 2 larger than the core masses in the P1 clump. It is quite possible that the mass of cores and protostars in the P1 region will grow through infall and become similar to those in the P2 region. Assuming that the cores in P2 is a few 10^5 yrs, the infall rate required for the core mass growth is a few times $10^{-4} M_\odot \text{ yr}^{-1}$. Such a high infall rate is consistent with expected infall rate $\frac{a^3}{G}$, where $a = 1.7 \text{ km s}^{-1}$ is the turbulent line width, and G is the gravitational constant. The mass accretion to the star, however, is likely to be much smaller as constrained by the low luminosity of $< 10^2 L_\odot$. Our observations of the P1 and P2 clumps suggest massive star formation through a low to intermediate mass phase as seen in P1 where masses of cores and protostars continue to grow via infall and accretion. More observations of similar regions are needed to test this scenario.

4. Conclusion

We carried out SMA observations of two massive clumps P1 and P2 which are at very different evolutionary stages. The main findings are:

- (1) The P1 clump is resolved into five cores at a projected separation of 0.19 pc, and masses much larger than the Jeans mass. The large masses indicates that turbulence and/or magnetic fields play important role in fragmentation;
- (2) The CO is depleted by a factor up to 10^3 in the P1 cores at a scale of $> 0.07\text{pc}$, much larger than the depletion area in low mass cores;
- (3) These findings indicate that the initial conditions assumed in current theoretical models should be amended in light of these observations.

Table 1: Physical Parameters in Cores

Name	R.A.(J2000) (<i>h m s</i>)	Dec.(J2000) (<i>° ' "</i>)	S (mJy)	T (K)	Mass (M_{\odot})	ΔV (km s^{-1})	M_J^a (M_{\odot})	M_V^b (M_{\odot})
P2-SMA1	18:42:51.98	-03:59:54.0	0.26	30	97	3.5	0.45	103
P2-SMA2	18:42:52.12	-03:59:54.2	0.13	30	49	3.5	0.45	103
P1-SMA1	18:42:51.18	-04:03:06.9	0.034	13	38	1.7	0.16	24
P1-SMA2	18:42:50.82	-04:03:11.3	0.030	16	27	1.7	0.16	24
P1-SMA3	18:42:50.58	-04:03:16.1	0.029	13	32	1.7	0.28	24
P1-SMA4	18:42:50.30	-04:03:20.3	0.057	13	64	1.7	0.19	24
P1-SMA5	18:42:49.82	-04:03:25.3	0.020	13	22	1.7	0.34	24

^aJeans masses are computed using the average density and temperature in the clumps.

^bViral masses are computed using a core radius of 0.02pc.

Fig. 1: The integrated intensity of the combined NH_3 (1,1) emission in white solid contours overlaid on the Spitzer 8 μm image in logarithmic color scales (Wang et al. 2008). The NH_3 image is contoured at 10% of the peak ($1 \text{ Jy beam}^{-1} \times \text{km s}^{-1}$). The star symbols mark the 24 μm emission peaks observed with MIPS/*Spitzer*. The cross symbols mark water maser emission detected with the VLA. The thin dashed line indicates the 50% of the sensitivity level of the 7 pointing mosaic in NH_3 . The NH_3 data have a resolution of $5'' \times 3''$, shown as the shaded ellipse at the lower-left corner of the panel. The thick dashed circles mark the SMA fields observed in this work.

Fig. 2: The dust continuum emission at 1.2mm from the IRAM 30m telescope, at 1.3mm (225 GHz) from the SMA, and NH_3 (1,1) integrated flux toward P1 and P2 clumps. The 1.2mm continuum emission from IRAM is contoured at 10% of the dust peak (1.3 Jy beam^{-1} in P2, and $0.26 \text{ Jy beam}^{-1}$ in P1). The 1.3mm continuum emission is contoured in steps of 20 mJy beam^{-1} for P2 and 5 mJy for P1. The NH_3 emission is contoured in steps of $50 \text{ mJy beam}^{-1} \text{ km s}^{-1}$. The shaded ellipses at the lower left corner of each panel is the resolution of the observations.

Fig. 3: The spectra from the 2GHz pandpass in the LSB and USB toward the dust cores P1-SMA4 and P2-SMA1.

Fig. 4: Visibility amplitude averaged over a concentric annulus versus UV distance in the P1-SMA4 and P2-SMA1 cores. The solid line is a least-squared fit to the data.

Fig. 1.—

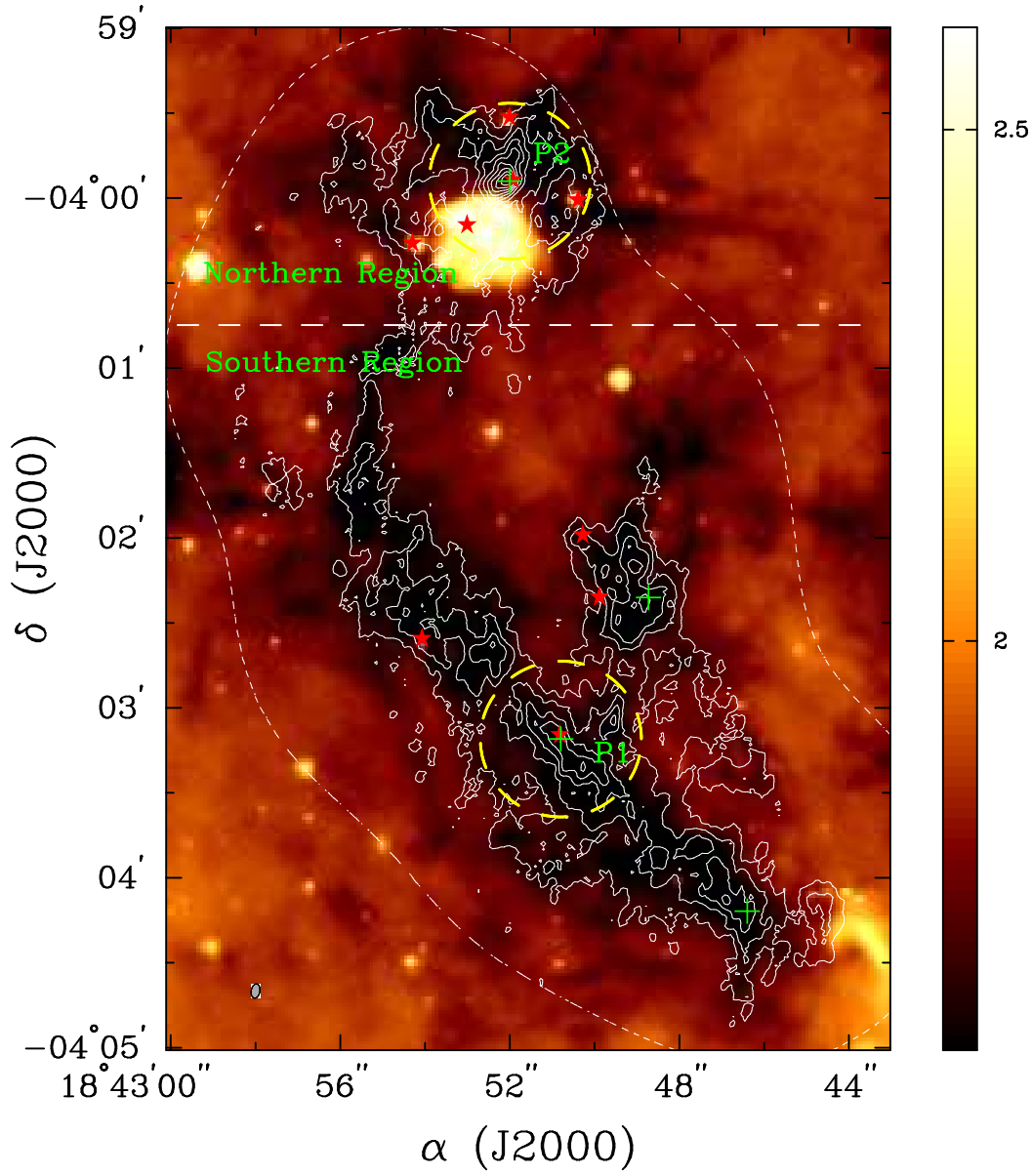


Fig. 2.—

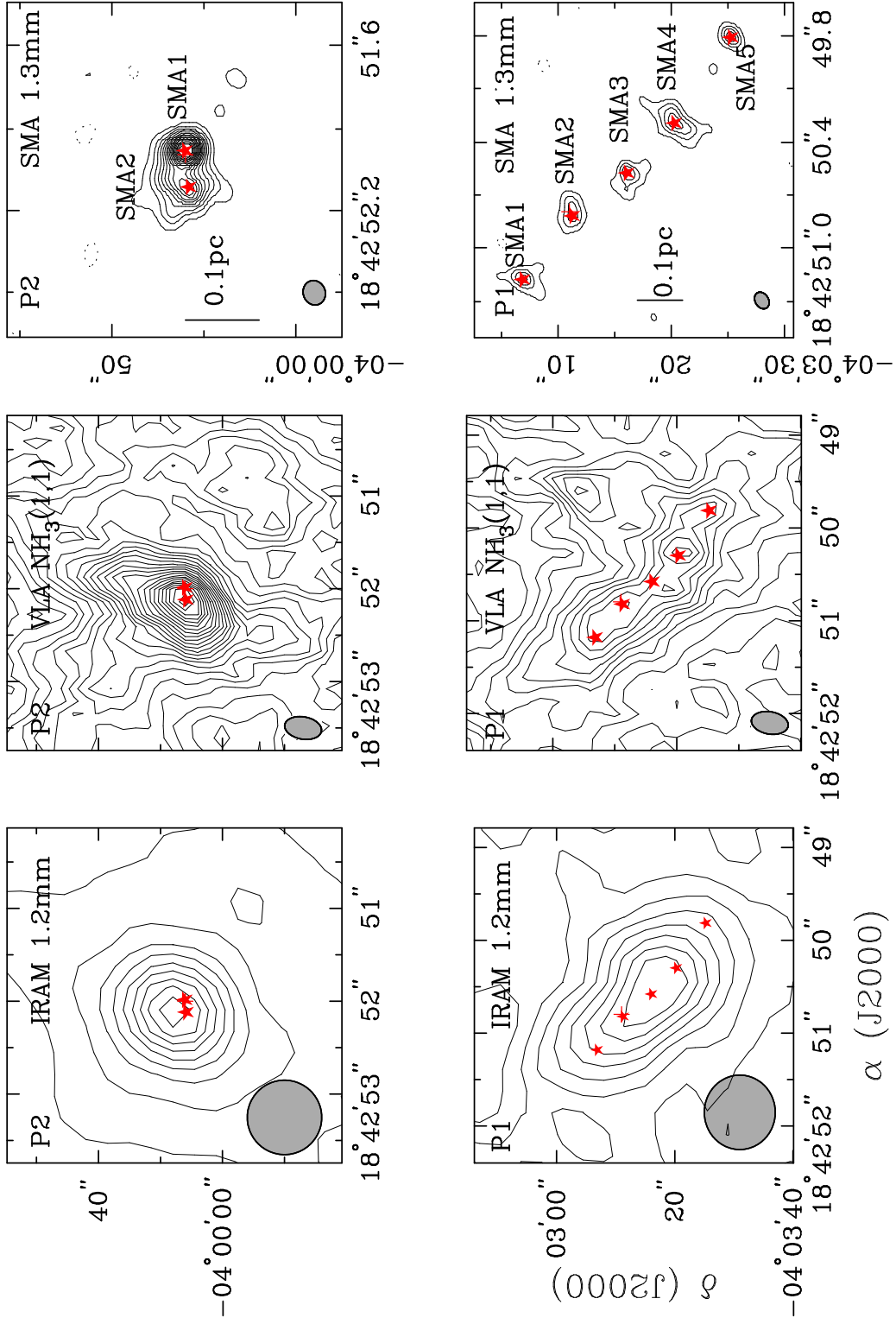


Fig. 3a.—

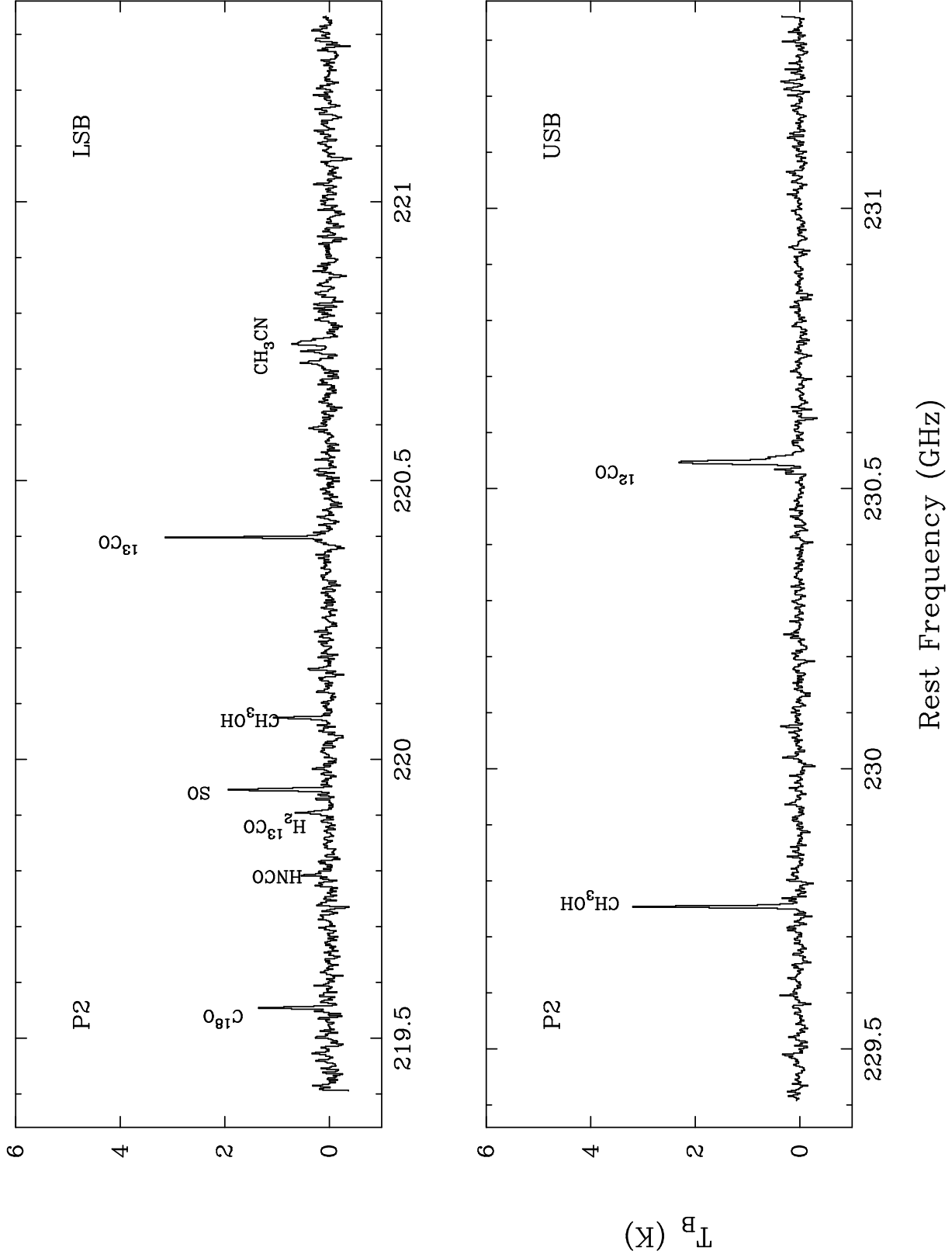


Fig. 3b.—

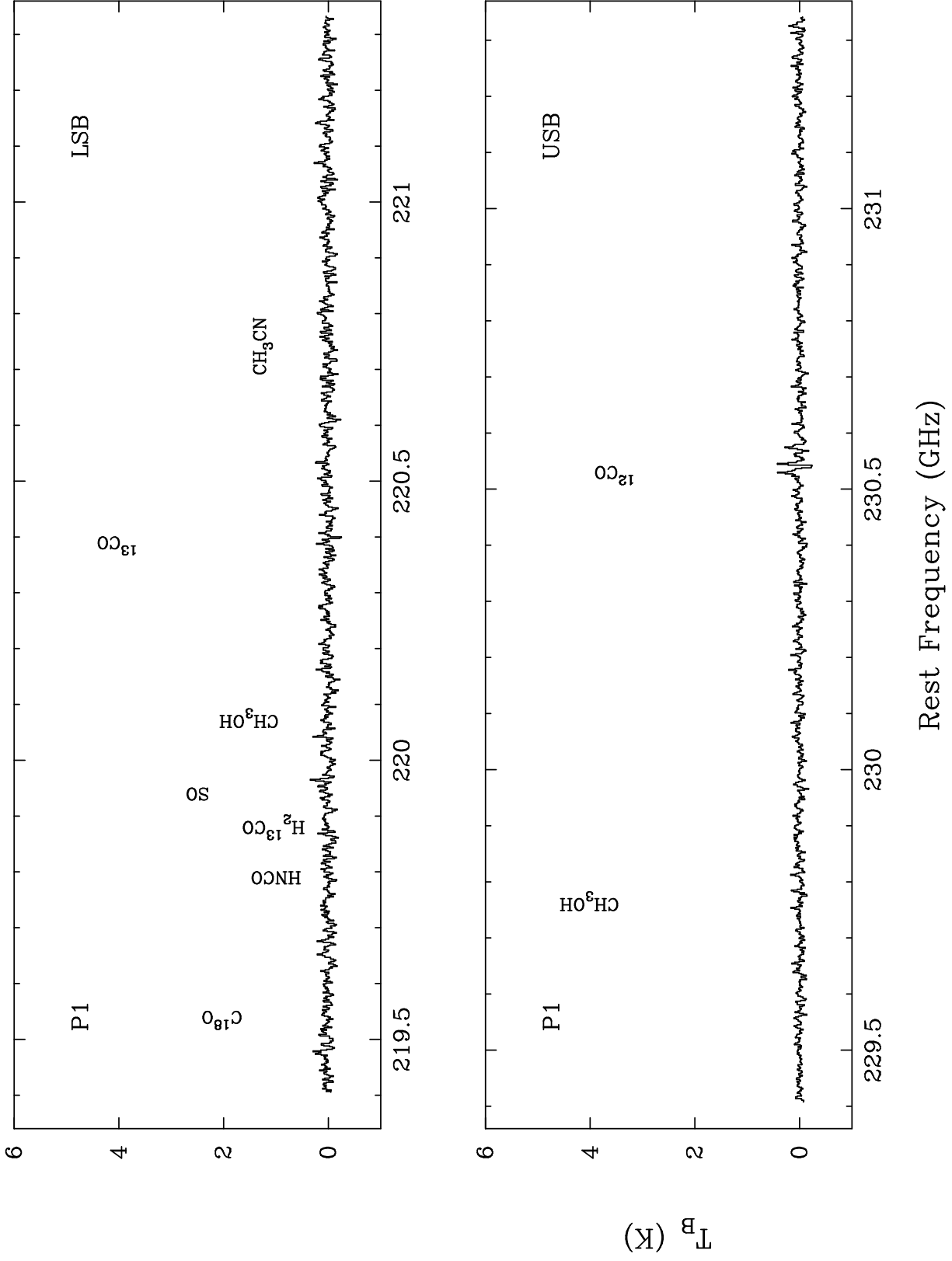
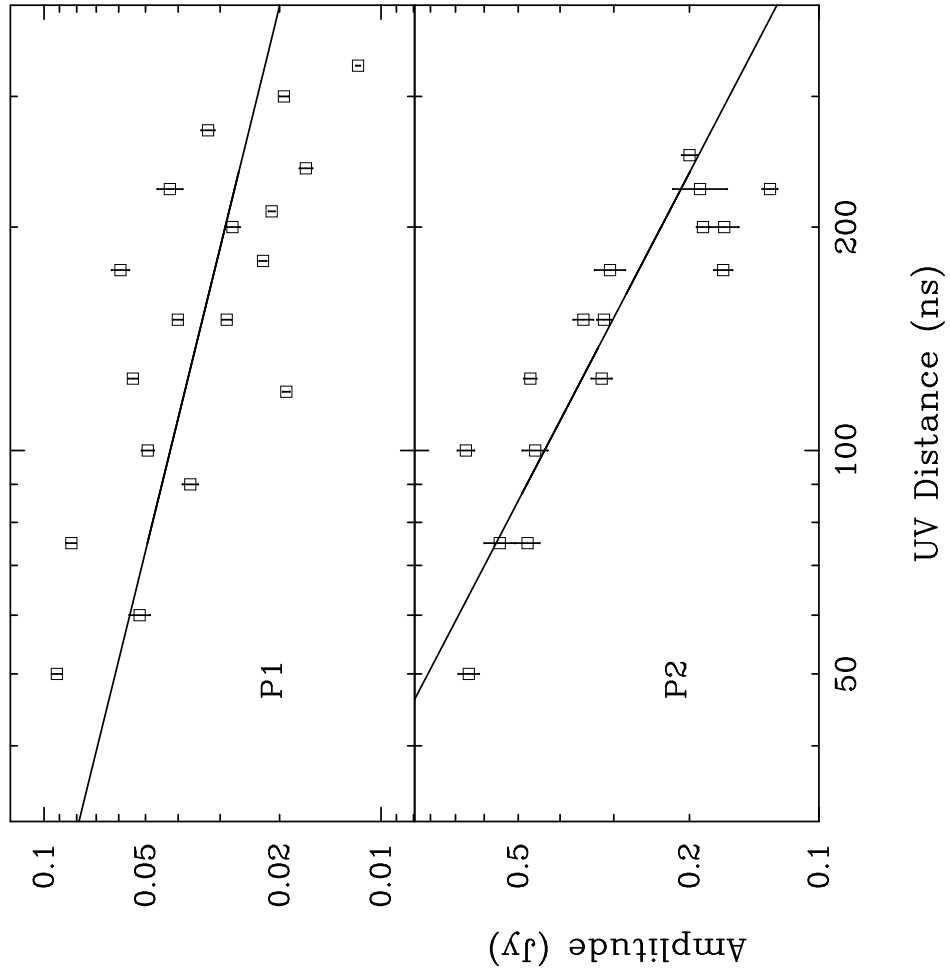


Fig. 4.—



REFERENCES

- Alves, J. F., Lada, C. J., & Lada, E. A. 2001, *Nature*, 409, 159
- Bergin, E. A. & Tafalla, M. 2007, *ARA&A*, 45, 339
- Beuther, H., Leurini, S., Schilke, P., et al. 2007, *A&A*, 466, 1065
- Beuther, H., Schilke, P., Sridharan, T. K., et al. 2002, *A&A*, 383, 892
- Beuther, H. & Sridharan, T. K. 2007, *ApJ*, 668, 348
- Beuther, H., Zhang, Q., Greenhill, L. J., et al. 2005, *ApJ*, 632, 355
- Bonnell, I. A. & Bate, M. R. 2002, *MNRAS*, 336, 659
- . 2005, *MNRAS*, 362, 915
- Bonnell, I. A., Vine, S. G., & Bate, M. R. 2004, *MNRAS*, 349, 735
- Carey, S. J., Clark, F. O., Egan, M. P., et al. 1998, *ApJ*, 508, 721
- Carey, S. J., Feldman, P. A., Redman, R. O., et al. 2000, *ApJ*, 543, L157
- Cesaroni, R., Felli, M., Testi, L., Walmsley, C. M., & Olmi, L. 1997, *A&A*, 325, 725
- Cesaroni, R., Galli, D., Lodato, G., Walmsley, C. M., & Zhang, Q. 2007, in *Protostars and Planets V*, ed. B. Reipurth, D. Jewitt, & K. Keil, 197–212
- Egan, M. P., Shipman, R. F., Price, S. D., et al. 1998, *ApJ*, 494, L199
- Ellingsen, S. P. 2006, *ApJ*, 638, 241
- Hennebelle, P., Péroult, M., Teyssier, D., & Ganesh, S. 2001, *A&A*, 365, 598
- Hildebrand, R. H. 1983, *QJRAS*, 24, 267
- Ho, P. T. P., Moran, J. M., & Lo, K. Y. 2004, *ApJ*, 616, L1
- Keto, E. 2002a, *ApJ*, 568, 754
- . 2002b, *ApJ*, 580, 980
- Krumholz, M. R. 2006, *ApJ*, 641, L45
- Krumholz, M. R., Klein, R. I., & McKee, C. F. 2007, *ApJ*, 656, 959

- Krumholz, M. R., McKee, C. F., & Klein, R. I. 2005, *Nature*, 438, 332
- Lada, C. J. & Lada, E. A. 2003, *ARA&A*, 41, 57
- Looney, L. W., Mundy, L. G., & Welch, W. J. 2000, *ApJ*, 529, 477
- McKee, C. F. & Tan, J. C. 2002, *Nature*, 416, 59
- Pillai, T., Wyrowski, F., Carey, S. J., & Menten, K. M. 2006, *A&A*, 450, 569
- Pillai, T., Wyrowski, F., Hatchell, J., Gibb, A. G., & Thompson, M. A. 2007, *A&A*, 467, 207
- Rathborne, J. M., Jackson, J. M., Chambers, E. T., et al. 2005, *ApJ*, 630, L181
- Rathborne, J. M., Jackson, J. M., & Simon, R. 2006, *ApJ*, 641, 389
- Rathborne, J. M., Jackson, J. M., Zhang, Q., & Simon, R. 2008, *ArXiv e-prints*
- Scoville, N. Z. & Kwan, J. 1976, *ApJ*, 206, 718
- Simon, R., Jackson, J. M., Rathborne, J. M., & Chambers, E. T. 2006a, *ApJ*, 639, 227
- Simon, R., Rathborne, J. M., Shah, R. Y., Jackson, J. M., & Chambers, E. T. 2006b, *ApJ*, 653, 1325
- Sollins, P. K., Zhang, Q., Keto, E., & Ho, P. T. P. 2005, *ApJ*, 624, L49
- van der Tak, F. F. S., van Dishoeck, E. F., Evans, II, N. J., & Blake, G. A. 2000, *ApJ*, 537, 283
- Wang, Y., Zhang, Q., Pillai, T., Wyrowski, F., & Wu, Y. 2008, *ApJ*, 672, L33
- Wang, Y., Zhang, Q., Rathborne, J. M., Jackson, J., & Wu, Y. 2006, *ApJ*, 651, L125
- Zhang, Q. 2005, in *IAU Symposium*, ed. R. Cesaroni, M. Felli, E. Churchwell, & M. Walm-
sley, 135–144
- Zhang, Q., Hunter, T. R., Beuther, H., et al. 2007, *ApJ*, 658, 1152
- Zhang, Q., Hunter, T. R., Brand, J., et al. 2001, *ApJ*, 552, L167
- Zhang, Q., Hunter, T. R., & Sridharan, T. K. 1998, *ApJ*, 505, L151